Eur. Phys. J. B (2018) 91: 11
https://doi.org/10.1140/epjb/e2017-80444-5

THE EUROPEAN PHYSICAL JOURNAL B

Regular Article

A torsional potential for graphene derived from fitting to DFT results

Georgios D. Chatzidakis[1], George Kalosakas[2,3], Zacharias G. Fthenakis[4,5], and Nektarios N. Lathiotakis[6,a]

[1] Department of Physics, National Technical University of Athens, 15780 Athens, Greece
[2] Materials Science Department, University of Patras, 26504 Rio, Greece
[3] Crete Center for Quantum Complexity and Nanotechnology (CCQCN), Physics Department, University of Crete, 71003 Heraklion, Greece
[4] Institute of Electronic Structure and Laser, FORTH, Heraklion, Greece
[5] Department of Physics, University of South Florida, Tampa, FL 33620, USA
[6] Theoretical and Physical Chemistry Institute, National Hellenic Research Foundation, Vass. Constantinou 48, 11635 Athens, Greece

Received 29 July 2017 / Received in final form 31 October 2017
Published online 17 January 2018 – © EDP Sciences, Società Italiana di Fisica, Springer-Verlag 2018

Abstract. We present a simple torsional potential for graphene to accurately describe its out-of-plane deformations. The parameters of the potential are derived through appropriate fitting with suitable DFT calculations regarding the deformation energy of graphene sheets folded around two different folding axes, along an armchair or along a zig-zag direction. Removing the energetic contribution of bending angles, using a previously introduced angle bending potential, we isolate the purely torsional deformation energy, which is then fitted to simple torsional force fields. The presented out-of-plane torsional potential can accurately fit the deformation energy for relatively large torsional angles up to 0.5 rad. To test our proposed potential, we apply it to the problem of the vertical displacement of a single carbon atom out of the graphene plane and compare the obtained deformation energy with corresponding DFT calculations. The dependence of the deformation energy on the vertical displacement of the pulled carbon atom is indistinguishable in these two cases, for displacements up to about 0.5 Å. The presented potential is applicable to other sp^2 carbon structures.

1 Introduction

Following the isolation of single layer graphene [1] an enormous research effort has been devoted to the study of this two-dimensional material and its properties [2–5]. Potential applications have been explored in electronics [6], opto-electronics [7], gas filtering [8], energy storage [9], uses related to its unique mechanical properties [10–12], etc.

Many empirical force fields have been used in atomistic simulations, calculating various structural, mechanical or phonon properties of graphene [13–23]. Besides the older, well known Tersoff [24,25] and Brenner [26] potentials, more accurate force fields have been introduced the last two decades. For example, optimized parameter sets for the latter potentials, providing better description of structural and phonon properties of graphene are presented in reference [27]. LCBOP [28,29] and AIREBO [30] are efficient potentials that have been widely applied in many calculations. Other potentials leading to good predictions of elastic and thermal properties of graphene have been also discussed [31].

More recently, we have presented simple analytical expressions for the accurate description of bond stretching and angle bending potentials of graphene [12]. These potentials are derived by fitting analytical functions to the deformation energy of proper distortions of graphene, obtained through accurate calculations from first principles' methods (DFT). The presented force field is applicable only to distortions restricted within the plane of graphene. These in-plane potentials can accurately describe elastic properties and the mechanical response of graphene in various extensional loads [12]. In this work, using similar ideas and methods, we extend this force field with torsional energy terms, in order to be able to describe out-of-plane distortions in graphene. The basic motivation is to provide a simple and computationally efficient classical potential which can be used for accurate large-scale atomistic calculations. The torsional potential presented here is also capable to describe other non-planar sp^2 carbon systems, like fullerenes and carbon nanotubes [32].

In the present work, we describe in detail the procedure followed and the necessary analytical calculations in order to fit the proposed torsional potential to ab-initio data. The full potential is then tested in the case of the deformation energy due to the vertical displacement

[a] e-mail: lathiot@eie.gr

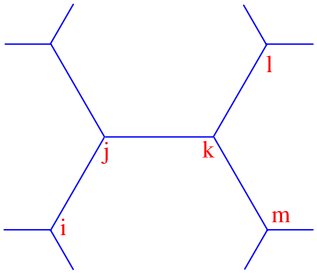

Fig. 1. Graphene's honeycomb lattice with a few atomic positions labeled as i, j, k, l, m.

of a carbon atom outside graphene's plane. Additional applications in realistic systems are presented in reference [32]. As shown there, the full proposed potential reproduces successfully the energetics of fullerenes, the strain energy and the Young modulus of carbon nanotubes, and the phonon dispersion of graphene, especially the out-of-plane, ZA, and ZO, branches that are directly related to the torsional terms introduced here. In this work, we have considered two types of folding of graphene sheets around different axes (either an armchair or a zig-zag one). The corresponding deformation energies are calculated using DFT methods. Following the removal of the contribution of angle bending terms in the total deformation energy, we isolated the pure torsional energy. Then, the analytic modeling of this energy in terms of individual torsional contributions, leads to a fitting procedure providing the optimal parameters of the out-of-plane torsional energy.

This paper is organized as follows: In Section 2, we describe the structures and methodology adopted for the DFT simulations that was used to obtain the deformation energies. Then in Section 3, we present the analytic calculations for removing the angle bending contributions from the deformation energies. The analytic expressions of the torsional energy in terms of the folding angles are provided in Section 4. The fitting of the torsional terms for two models considered here is described in Section 5, completing the presentation of the derivation of the new torsional force fields. Then, in Section 6, we present a test case, the deformation energy due to the vertical displacement of a carbon atom outside graphene's plane, as an application of the proposed scheme and compare the predictions with DFT results. Finally, a summary and conclusions are given in Section 7.

2 Structures and DFT calculations

2.1 Torsional angles in graphene

In Figure 1, we show a part of the honeycomb structure of graphene and a few carbon-atom positions labeled as i, j, k, l, m. The quadruple (i, j, k, l), with three of these positions belonging to the same hexagonal ring and one to an adjacent is customary called *trans*, while the quadruple (i, j, k, m), with all belonging to the same ring, is called *cis*. In the case that the structure is distorted and the atoms in the quadruple (i, j, k, l) are no longer co-planar, we can define a torsional angle, which we label (i-j-k-l), as the dihedral angle of the planes i-j-k and j-k-l. The torsional angles can then be classified as *trans* or *cis* accordingly. The dihedral angle between two planes, e.g. i-j-k and j-k-l, can be defined as the angle between the vectors perpendicular to the planes. We assumed that the perpendicular vectors are pointing inwards for clockwise triples (like i-j-k) or outwards for anti-clockwise triples (like j-k-l). Under this assumption, torsional angles are in the range $[0, \pi]$ with *cis* angles smaller than $\pi/2$ and *trans* angles larger than $\pi/2$.

2.2 DFT results

DFT calculations were performed for two distorted graphene structures: one that graphene is folded around an armchair axis and one around a zig-zag. These structures are shown in Figure 2 where we label all atoms relevant to the present discussion. They are periodic along the folding axis, while on the vertical direction they are not. The folding angle around either the armchair or zig-zag axis is denoted by ϕ. Throughout the paper we denote with symbol θ "usual" angles between carbon bonds (bending angles) and with ω torsional (dihedral) angles as defined in the previous subsection.

All ab initio calculations were performed with Quantum-Espresso periodic-DFT code [33], with the same pseudopotential [34] as in reference [12]. The wavefunction and density plane-wave cutoffs were chosen 40 Ry and 400 Ry, respectively. The unit cell we chose is minimal in the periodic direction (that of the folding axis) while, in the vertical direction, it is appropriately large to avoid edge-effects. Thus, the simulated structures are nanoribbons that are folded around their middle line axis. In the case of the armchair folding (Fig. 2, top), the unit cell is such that neighbors up to the 5th in the vertical direction were included. In the case of the zig-zag folding the corresponding dimension is long enough to include up to 8th neighbors. Thus, the unit cells contain 22 and 17 atoms for the armchair and the zig-zag folding axes, respectively. In the reciprocal space, we used a mesh of $1 \times 24 \times 1$, i.e. 24 points were assumed along the bending direction that the structure is periodic.

In Figure 3, we show with filled circles the DFT calculated total deformation energy per unit cell along the folding direction, as a function of the folding angle ϕ, for both armchair and zig-zag folding actions, $E_d^{(\mathrm{a})}$ and $E_d^{(\mathrm{z})}$, respectively. The total deformation energy per unit-cell is taken as the energy difference between the folded structure and the planar one ($\phi = 0$). Apparently, the two structural distortions due to the considered foldings are composite and consist of several individual angle-bending and torsional deformations. Note that bond lengths are not altered, so there is no bond-stretching contribution in the total deformation energy.

In order to perform a fitting for the torsional terms alone, we first need to exclude angle-bending contributions from the total deformation energy. To this end, we (i) identify all angle-bending terms and express analytically their corresponding bending angles θ in terms of ϕ and then (ii) remove the angle-bending terms using the analytic

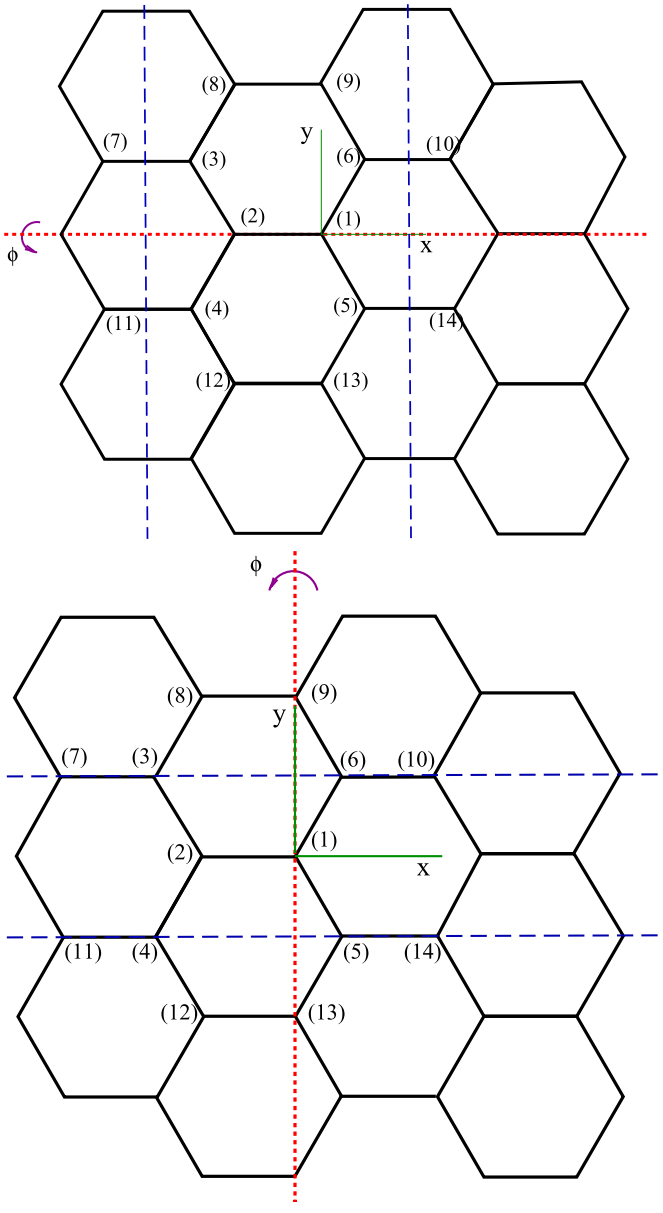

Fig. 2. Part of graphene's structure with the armchair (top) and zig-zag (bottom) folding axes shown by dotted lines. We label several atoms that are mentioned in the text. The structure is periodic along the bending axis direction. The boundaries of the unit cell, adopted in the DFT calculations, in the folding direction are shown by the vertical dashed blue lines. The size in the vertical to the folding direction is described in the text.

potential presented in reference [12]. The residual, pure torsional energy per unit cell, when the contribution from angle-bending is subtracted, as a function of the out-of-plane folding angle ϕ is shown in Figure 3 (diamonds), for the two different folding directions. As we see in Figure 3, the contribution from angle bending is significant for ϕ larger than 0.2 rad. In order to fit an analytic expression to the torsional terms, we have to (i) identify all the individual torsional terms that contribute to the pure torsional energy for each of the zig-zag and armchair folding cases,

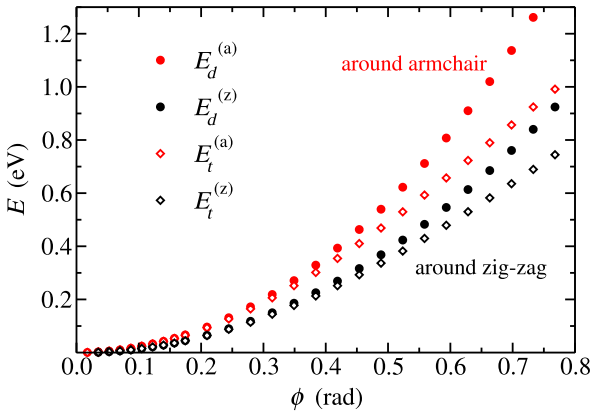

Fig. 3. The total deformation energies, $E_d^{(a)}$ and $E_d^{(z)}$, calculated with DFT (filled circles) and the pure torsional energies, $E_t^{(a)}$ and $E_t^{(z)}$, after removing angle bending terms (diamonds), as a function of the folding angle ϕ. The superscripts (a) and (z) correspond to the armchair (red) and zig-zag (black) folding cases, respectively.

and, subsequently (ii) express the corresponding torsional angles in terms of the folding angle, ϕ. These steps are described in the following two sections, where all necessary analytical expressions are presented.

3 Removing the angle-bending terms

3.1 Folding around the armchair axis

In the case of folding around the armchair direction (Fig. 2, top) two atoms of the unit-cell lie on the folding axis (labeled 1 and 2). It is easy to see that the folding alters two of their bending angles per unit cell, $\widehat{(324)}$ and $\widehat{(615)}$, which are equal. One can show that these angles, in terms of ϕ, are given by

$$\theta^{(a)} = 2\arcsin\left(\sqrt{\frac{3}{8}}\sqrt{\cos\phi + 1}\right). \quad (1)$$

The angle-bending energy that one needs to remove from the total energy is

$$U_b^{(a)} = 2V_b(\theta^{(a)}(\phi)), \quad (2)$$

where $V_b(\theta)$ is obtained from the analytical expression for the angle-bending potential given in reference [12]:

$$V_b(\theta) = \frac{k}{2}\left(\theta - \frac{2\pi}{3}\right)^2 - \frac{k'}{3}\left(\theta - \frac{2\pi}{3}\right)^3, \quad (3)$$

with $k = 7.0$ eV/rad^2 and $k' = 4$ eV/rad^3.

Removing these terms from the total deformation energies, $E_d^{(a)}$, we find the total (pure) torsional energy

$$E_t^{(a)} = E_d^{(a)} - U_b^{(a)}, \quad (4)$$

shown in Figure 3.

3.2 Folding around the zig-zag axis

Similarly, in the case of folding around the zig-zag direction (Fig. 2, bottom) only one atom in the unit-cell (labeled 1), lies on the folding axis. The folding affects two of its angles, $\widehat{(216)}$ and $\widehat{(215)}$, that are also equal. In terms of ϕ, these angles are given by

$$\theta^{(\mathrm{z})} = 2\arcsin\left(\frac{1}{2}\sqrt{2+\cos\phi}\right). \tag{5}$$

Then, the angle-bending energy that one needs to subtract from the total energy is

$$U_b^{(\mathrm{z})} = 2V_b(\theta^{(\mathrm{z})}(\phi)). \tag{6}$$

Removing these terms from the total deformation energy, we find the pure torsional energy,

$$E_t^{(\mathrm{z})} = E_d^{(\mathrm{z})} - U_b^{(\mathrm{z})}, \tag{7}$$

presented in Figure 3 for this case.

4 Analytical expressions for the torsional energy

Here we provide analytical expressions for the total torsional energies , $U_t^{(\mathrm{a})}(\phi)$ and $U_t^{(\mathrm{z})}(\phi)$, as functions of the folding angle ϕ. These expressions contain parameters to be fitted so that they reproduce, as close as possible, the DFT derived $E_t^{(\mathrm{a})}$ and $E_t^{(\mathrm{z})}$ data shown in Figure 3. To arrive to such analytical expressions we first identify all altered torsional angles (per unit cell) and express them in terms of the folding angle ϕ. Then, $U_t^{(\mathrm{a})}(\phi)$ and $U_t^{(\mathrm{z})}(\phi)$ will be just the sum of all individual torsional terms that correspond to these altered torsional angles.

Regarding the individual torsional potential energy, $V_t(\omega)$, two different functional forms would be considered. The most frequently used formula, referred as model 1 here, is

$$V_t(\omega) = \frac{1}{2}V_1[1+\cos\omega] + \frac{1}{2}V_2[1-\cos(2\omega)]. \tag{8}$$

An alternative model, which we call model 2, assumes a different fitting formula for *cis* or *trans* dihedral angles ω

$$V_t^{\mathrm{cis}}(\omega) = K_{\mathrm{cis}}[1-\cos(2\omega)], \quad V_t^{\mathrm{trans}}(\omega) = K_{\mathrm{trans}}[1-\cos(2\omega)], \tag{9}$$

where either the first or the second expression of equation (9) is used for *cis* or *trans* torsional angles, respectively. Below we use both models 1 and 2 to fit their parameters to the obtained DFT results.

4.1 Folding around the armchair axis

Inspecting Figure 2 (top) we identify the following torsional (dihedral) angles per unit cell that are altered by folding around an axis along the armchair direction:

– 2 *trans* dihedral angles, (5-1-2-3), (4-2-1-6), with

$$\omega_1^{(\mathrm{a})}(\phi) = \arccos(-\cos\phi) \tag{10}$$

– 4 *cis* dihedral angles, (11-4-2-3), (14-5-1-6), (7-3-2-4), (10-6-1-5), with

$$\omega_2^{(\mathrm{a})}(\phi) = \arccos\left(\sqrt{3}\frac{1+\cos\phi}{\sqrt{9\sin^2\phi+6(1+\cos\phi)}}\right) \tag{11}$$

– 4 *trans* dihedral angles, (12-4-2-3), (13-5-1-6), (8-3-2-4), (9-6-1-5), with

$$\omega_3^{(\mathrm{a})}(\phi) = \arccos\left(-\sqrt{3}\frac{1+\cos\phi}{\sqrt{9\sin^2\phi+6(1+\cos\phi)}}\right) \tag{12}$$

Through the expressions given above, the total torsional energy, $U_t^{(\mathrm{a})}$ within the model 1, becomes an analytic function of ϕ:

$$U_t^{(\mathrm{a})}(\phi) = 2V_t(\omega_1^{(\mathrm{a})}(\phi)) + 4V_t(\omega_2^{(\mathrm{a})}(\phi)) + 4V_t(\omega_3^{(\mathrm{a})}(\phi)), \tag{13}$$

where $V_t(\omega)$ is the individual torsional term given in equation (8).

For the model 2, the corresponding expression of the total torsional energy $U_t^{(\mathrm{a})}$ is

$$U_t^{(\mathrm{a})}(\phi) = 2V_t^{\mathrm{trans}}(\omega_1^{(\mathrm{a})}(\phi)) + 4V_t^{\mathrm{cis}}(\omega_2^{(\mathrm{a})}(\phi)) + 4V_t^{\mathrm{trans}}(\omega_3^{(\mathrm{a})}(\phi)), \tag{14}$$

with V_t^{cis} and V_t^{trans} given by equation (9).

4.2 Folding around the zig-zag axis

From Figure 2 (bottom) we identify the following dihedral angles per unit cell that are affected by the folding around a zig-zag axis:

– 2 *cis* dihedral angles, (3-2-1-6), (4-2-1-5), with

$$\omega_1^{(\mathrm{z})}(\phi) = \arccos\left(\sqrt{\frac{3}{\sin^2\phi+3}}\right) \tag{15}$$

– 2 *trans* dihedral angles, (4-2-1-6), (3-2-1-5), with

$$\omega_2^{(z)}(\phi) = \arccos\left(-\sqrt{\frac{3}{\sin^2\phi + 3}}\right) \quad (16)$$

– 2 *cis* dihedral angles, (2-1-5-13), (2-1-6-9), with

$$\omega_3^{(z)}(\phi) = \arccos\left(\sqrt{\frac{3}{\sin^2\phi + 3}}\cos\phi\right) \quad (17)$$

– 2 *trans* dihedral angles, (2-1-5-14), (2-1-6-10), with

$$\omega_4^{(z)}(\phi) = \arccos\left(-\sqrt{\frac{3}{\sin^2\phi + 3}}\cos\phi\right) \quad (18)$$

Then the total torsional energy for the model 1 is given by

$$U_t^{(z)}(\phi) = 2V_t(\omega_1^{(z)}(\phi)) + 2V_t(\omega_2^{(z)}(\phi)) + 2V_t(\omega_3^{(z)}(\phi)) + 2V_t(\omega_4^{(z)}(\phi)), \quad (19)$$

while for the case of model 2 becomes

$$U_t^{(z)}(\phi) = 2V_t^{cis}(\omega_1^{(z)}(\phi)) + 2V_t^{trans}(\omega_2^{(z)}(\phi)) + 2V_t^{cis}(\omega_3^{(z)}(\phi)) + 2V_t^{trans}(\omega_4^{(z)}(\phi)). \quad (20)$$

5 Fitting procedure

The pure torsional energy data derived through DFT calculations, $(\phi_i, E_{t,i}^{(a)})$ and $(\phi_i, E_{t,i}^{(z)})$, shown with red and black diamonds respectively in Figure 3, and the analytical expressions $U_t^{(a)}$ and $U_t^{(z)}$ given in equations (13) and (19) for the model 1 (or Eqs. (14) and (20) for the model 2) can be used to obtain the optimal parameters V_1 and V_2 (or K_{cis} and K_{trans}) of the individual torsional terms so that $U_t^{(a)}$ and $U_t^{(z)}$ reproduce the dependence of $E_t^{(a)}(\phi)$ and $E_t^{(z)}(\phi)$ as close as possible. For this purpose, adopting a standard procedure, we minimize an objective function $OF(V_1, V_2)$ or $OF(K_{cis}, K_{trans})$ which is the equal-weighted sum of the square differences,

$$OF = \sum_{i=1}^{\phi_i<\phi_{max}} \left[E_{t,i}^{(a)} - U_t^{(a)}(\phi_i)\right]^2 + \sum_{i=1}^{\phi_i<\phi_{max}} \left[E_{t,i}^{(z)} - U_t^{(z)}(\phi_i)\right]^2. \quad (21)$$

The sums in the above expression run over all i for which ϕ_i is smaller than an upper-limit angle ϕ_{max}.

Table 1. Model 1: Optimal fitting parameters V_1 and V_2 for model 1, for the three different values of ϕ_{max} examined.

ϕ_{max} (°)	V_1 (eV)	V_2 (eV)
10	−0.00013	0.221
20	−0.00017	0.226
30	−0.00035	0.233

For the model 1, the fitted total torsional energies $U_t^{(a)}(\phi)$ and $U_t^{(z)}(\phi)$ given by equations (13) and (19) depend on V_1 and V_2 through the corresponding dependence of the individual torsional terms V_t of equation (8).

In the case of model 2, we optimize K_{cis} and K_{trans} parameters, and the expressions (14) and (20) are used instead, where the individual torsional terms V_t^{cis} or V_t^{trans} are given by equation (9).

The choice of ϕ_{max} is expected to affect the quality of fitting for small and large values of ϕ. We are interested in checking whether the fitting parameters depend on ϕ_{max} and, if so, at what extend.

5.1 Model 1: fitting results for V_1, V_2

We performed fitting of the parameters V_1 and V_2 of equation (8), for three different values of ϕ_{max}: 10°, 20° and 30°. The optimal parameters V_1 and V_2 are given in Table 1 for each case.

In Figure 4, we show, the total torsional energies, $E_t^{(a)}$ and $E_t^{(z)}$ and the fitted analytical expressions for these three values of ϕ_{max}. In all cases, the fitting reproduces the armchair data in closer agreement than the zig-zag, i.e. for a larger range of ϕ. For $\phi_{max} = 10°$, there is a rather good agreement for values of ϕ up to 0.50 rad for the armchair case and 0.40 rad for the zig-zag case. For $\phi_{max} = 20°$, this range of agreement increases roughly up to 0.60 rad and 0.45 rad for the armchair and zig-zag cases, respectively. Finally, for $\phi_{max} = 30°$, this agreement range increases further up to 0.70 and 0.50 rad, respectively. As expected, by increasing ϕ_{max}, the maximum range of agreement also increases, but this is at the cost of the agreement for smaller angles. As the fitting procedure is trying to fit better larger values of ϕ the quality for smaller angles deteriorates. This deterioration, however, is rather small as one can see in the insets of Figures 4a–4c where the region of smaller angles is enlarged.

However, in general, for angles ϕ up to 0.4 rad (22°) corresponding to torsional energies 0.2–0.3 eV, all fittings are satisfactory. On the other hand, as we see in Table 1, the fitted values of V_1 and V_2 are not so sensitive to the value of ϕ_{max}: V_1 remains close to zero while V_2 is in the range 0.22–0.23 eV. Further, the value of $V_2 = 0.23$ eV, obtained for $\phi_{max} = 20$–30° performs better for larger angles, up to 0.5 rad, corresponding to energies of 0.4–0.5 eV, while on the other hand the fitted results in the region of smaller ϕ remain satisfactory. These considerations suggest that it is quite reasonable to adopt as optimal parameters $V_1 = 0$ and $V_2 = 0.23$ eV. Thus, our proposed torsional potential

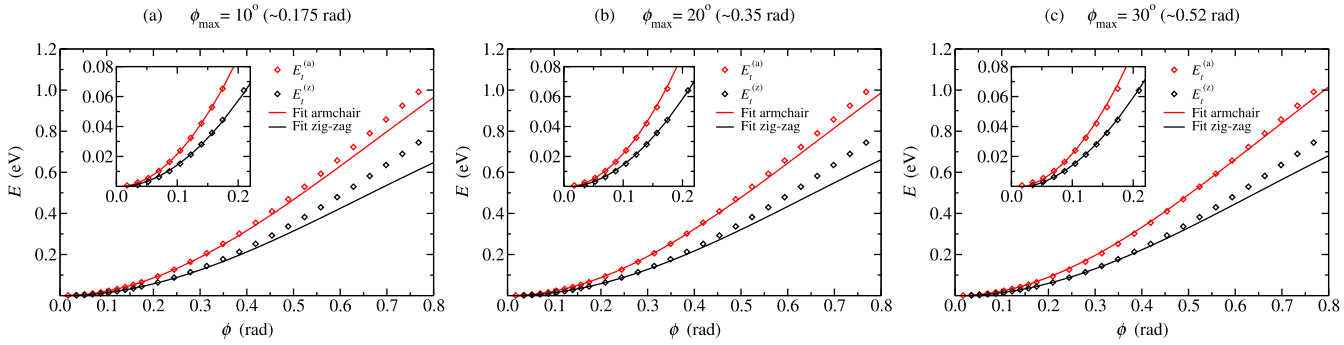

Fig. 4. Fit of the analytical expressions for **model 1** (lines) to the numerically derived data $E_t^{(a)}$ and $E_t^{(z)}$ (points) of the total torsional energy, for different choices of ϕ_{max} equal to (a) 10°, (b) 20°, and (c) 30°. In the inset we zoom in the region of small angles ϕ.

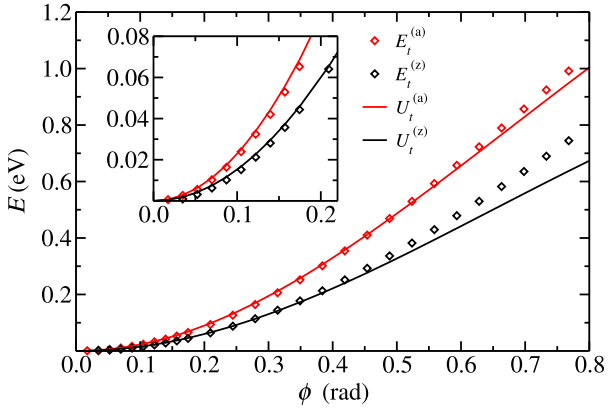

Fig. 5. The analytical torsional energies considering model 1, for the folding around the armchair (a) and zig-zag (z) axes, $U_t^{(a)}$ and $U_t^{(z)}$, equations (13) and (19) respectively, using the proposed parameters $V_1 = 0$ eV and $V_2 = 0.23$ eV (lines), compared to the numerically derived data $E_t^{(a)}$ and $E_t^{(z)}$ (points). The inset zooms in small values of ϕ to illustrate the quality of the fit in that region.

has the simple form

$$V_t(\omega) = \frac{1}{2} V_2 \left(1 - \cos(2\omega)\right), \quad V_2 = 0.23 \text{ eV}. \tag{22}$$

The analytical torsional energy using this potential is shown in Figure 5 along with the DFT derived $E_t^{(a)}$ and $E_t^{(z)}$ data.

5.2 Model 2: fitting results for K_{cis}, K_{trans}

As in the previous subsection, we performed the fitting of parameters K_{cis} and K_{trans} of equation (9) for the same values of ϕ_{max}, i.e. 10°, 20° and 30°. The optimal parameters K_{cis} and K_{trans} for each of these cases are given in Table 2. In Figure 6, we show the resulted fitting (lines) for the armchair and zig-zag folding cases for all three values of ϕ_{max}, compared to the DFT derived data for the total torsional energy per unit cell, $E_t^{(a)}$ and $E_t^{(z)}$ (points). The fitting quality is quite similar to that of the previous subsection. Again, for $\phi_{max} = 20°$ and 30°, the quality improves for larger values of ϕ and at the same time the fit for smaller ϕ does not deteriorate substantially. Thus, we propose a rounded optimal set $K_{cis} = 0.14$ eV and $K_{trans} = 0.10$ eV which is close to the values obtained for $\phi_{max} = 20°$ and 30°. In Figure 7, we show the torsional energy analytically obtained with model 2 using these values for K_{cis} and K_{trans}, compared with the numerical data $E_t^{(a)}$ and $E_t^{(z)}$.

Table 2. Model 2: Optimal fitting parameters K_{cis} and K_{trans}, for the three different values of ϕ_{max} examined.

ϕ_{max} (°)	K_{cis} (eV)	K_{trans} (eV)
10	0.104	0.112
20	0.134	0.096
30	0.150	0.090

To summarize, for the model 2, we propose

$$V_t^{cis}(\omega) = K_{cis}[1 - \cos(2\omega)], \; K_{cis} = 0.14 \text{ eV},$$
$$V_t^{trans}(\omega) = K_{trans}[1 - \cos(2\omega)], \; K_{trans} = 0.10 \text{ eV}, \tag{23}$$

where either the former or the latter expression is used depending on whether the torsional angle ω is *cis* or *trans*, respectively.

5.3 Comparison of the two models

In Figure 8, we show the total torsional energies per unit cell, for both fitting forms of models 1 and 2, using the optimal parameters obtained previously. Note that the two models are of the same quality. They almost coincide for the armchair case, while for the zig-zag one, the model 2 is slightly better for larger ϕ's and the model 1 marginally better for smaller ones. The differences however are not significant for ϕ's up to 0.5 rad.

The obtained optimal parameters of model 2, $K_{cis} = 0.14$ eV and $K_{trans} = 0.10$ eV, are close to each other, indicating that a single parameter with value the average of them would offer a reasonable description. Moreover, this average value is almost equal to $V_2/2$. Thus, it is rather unnecessary to assume different parameters for *cis* and

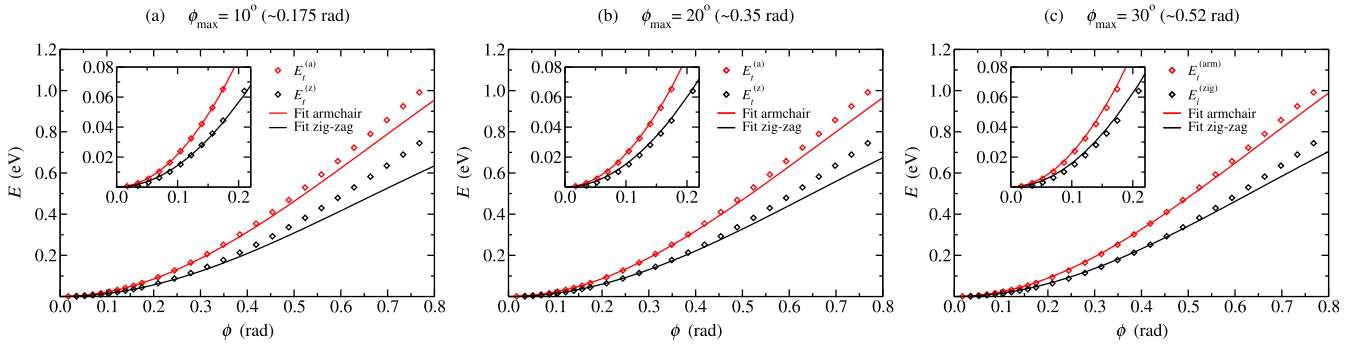

Fig. 6. Fit of the analytical expressions for **model 2** (lines) to the numerically derived data $E_t^{(a)}$ and $E_t^{(z)}$ (points) of the total torsional energy, for different choices of ϕ_{max} equal to (a) 10°, (b) 20°, and (c) 30°. In the inset we zoom in the region of small angles ϕ.

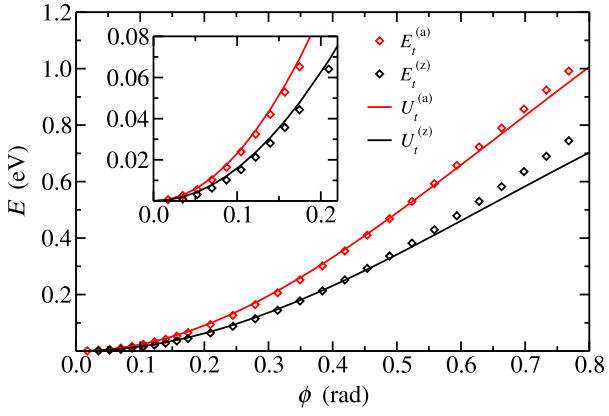

Fig. 7. The analytical torsional energies considering model 2, for the folding around the armchair (a) and zig-zag (z) axes, $U_t^{(a)}$ and $U_t^{(z)}$, equations (14) and (20) respectively, using the proposed parameters $K_{cis} = 0.14\,eV$ and $K_{trans} = 0.10\,eV$ (lines), compared to the DFT derived data $E_t^{(a)}$ and $E_t^{(z)}$ (points). The inset zooms in small values of ϕ to illustrate the quality of the fit in that region.

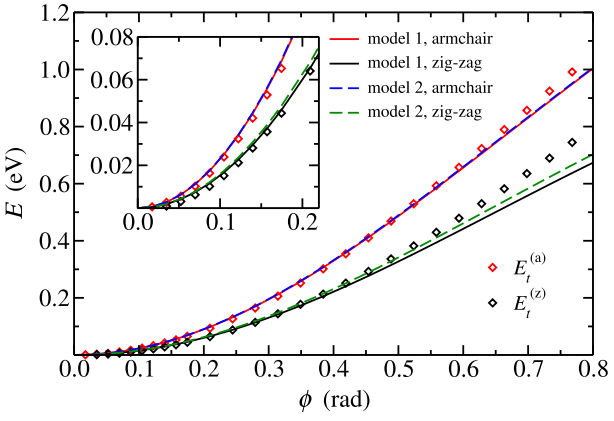

Fig. 8. Comparison between the fitting of the two models: model 1 with parameter values $V_1 = 0\,eV$, $V_2 = 0.23\,eV$ and model 2 with parameters $K_{cis} = 0.14\,eV$, $K_{trans} = 0.10\,eV$.

trans dihedral angles and, to keep things as simple as possible, the simple form of equation (22), is quite sufficient to describe all torsional distortions. Therefore, the model 1 of equation (22) is our proposed one, containing a single parameter V_2.

6 Application to the vertical displacement of a carbon atom in graphene

In order to test the accuracy of the proposed parameters for the torsional terms, we consider the deformation energy of graphene due to a vertical, out-of-plane displacement of a single carbon atom. We consider that apart from the vertically displaced atom, all other atoms remain fixed at their equilibrium positions within graphene's plane. The task is to compare the deformation energy obtained by the present potential, along with the in-plane force field of reference [12], with that obtained by DFT calculations (using the same method that was used to produce the data discussed above).

The process of moving a carbon atom vertically outside graphene's plane is described by a deformation energy consisting of all kinds of individual potential energy terms, i.e. bond-stretching, angle-bending and of course torsional terms.

Concerning the bond-stretching terms, the vertical movement of a carbon atom at a displacement z over the plane, alters only the three bonds of that atom (see Fig. 9). If the length of these bonds at $z = 0$ is d their altered length d' becomes

$$d'(z) = \sqrt{d^2 + z^2}. \tag{24}$$

At the same time, two different kinds of angle-bending terms appear corresponding to: (i) the three angles, θ_1, between the atom's bonds (marked in red in Fig. 9) and (ii) the six angles, θ_2, between these bonds and the bonds marked in blue in Figure 9. These angles can be expressed in terms of the displacement z as

$$\theta_1(z) = \arccos\left(\frac{2z^2 - d^2}{2(d^2 + z^2)}\right) \tag{25}$$

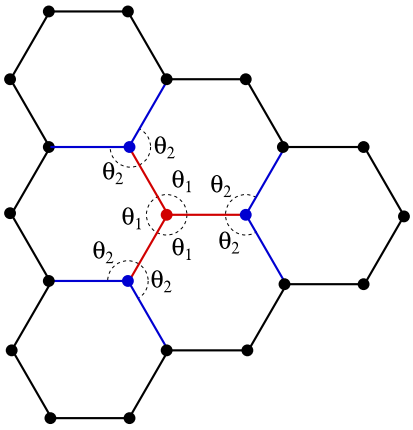

Fig. 9. A vertical displacement (normal to the page) of a carbon atom (marked red) results in contributions to the total deformation energy from bond-stretching (elongation of red bonds), angle-bending (altering θ_1 and θ_2 angles), and torsional terms (twisting around red and blue bonds).

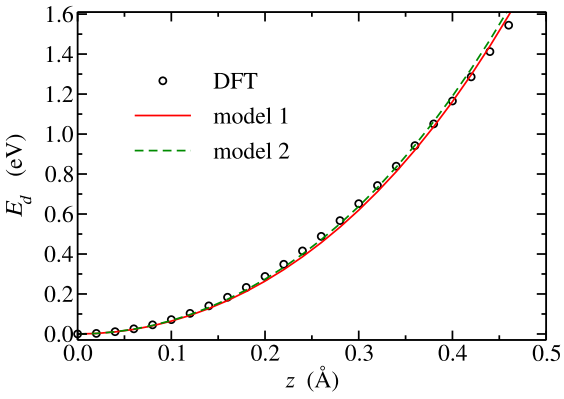

Fig. 10. The deformation energy, E_d, written in analytical form in equation (31), due to the vertical out-of-plane displacement of a single carbon atom in graphene as a function of the vertical displacement z, calculated with the present potential and compared to DFT results.

and

$$\theta_2(z) = \arccos\left(-\frac{d}{2\sqrt{d^2+z^2}}\right). \tag{26}$$

Finally, several torsional terms also contribute to the deformation energy. There are rotations around the 3 bonds of the displaced atom and its first neighbors (marked in red in Fig. 9) as well as rotations around the 6 bonds of the first neighbors and the second neighbors (marked in blue in Fig. 9). These rotations correspond to the following torsional angles:

– 6 *cis* dihedral angles around the bonds marked in red in Figure 9 given by

$$\omega_{\rm cis}^{(1)}(z) = \arccos\left(\frac{\frac{3}{4}}{\sqrt{\left(\frac{z}{d}\right)^2+\frac{3}{4}}\sqrt{3\left(\frac{z}{d}\right)^2+\frac{3}{4}}}\right) \tag{27}$$

– 6 *trans* dihedral angles around the bonds marked in red in Figure 9 given by

$$\omega_{\rm trans}^{(1)}(z) = \arccos\left(\frac{-\frac{3}{2}\left(\frac{z}{d}\right)^2-\frac{3}{4}}{\sqrt{\left(\frac{z}{d}\right)^2+\frac{3}{4}}\sqrt{3\left(\frac{z}{d}\right)^2+\frac{3}{4}}}\right) \tag{28}$$

– 6 *cis* dihedral angles around the bonds marked in blue in Figure 9 given by

$$\omega_{\rm cis}^{(2)}(z) = \arccos\left(\frac{1}{\sqrt{\frac{4}{3}\left(\frac{z}{d}\right)^2+1}}\right) \tag{29}$$

– 6 *trans* dihedral angles around the bonds marked in blue in Figure 9 given by

$$\omega_{\rm trans}^{(2)}(z) = \arccos\left(\frac{-1}{\sqrt{\frac{4}{3}\left(\frac{z}{d}\right)^2+1}}\right). \tag{30}$$

Then, the total deformation energy is given by

$$\begin{aligned} E_d(z) = {} & 3V_s(d'(z)) + 3V_b(\theta_1(z)) + 6V_b(\theta_2(z)) \\ & + 6V_t(\omega_{\rm cis}^{(1)}(z)) + 6V_t(\omega_{\rm trans}^{(1)}(z)) \\ & + 6V_t(\omega_{\rm cis}^{(2)}(z)) + 6V_t(\omega_{\rm trans}^{(2)}(z)), \end{aligned} \tag{31}$$

where $V_s(r)$, $V_b(\theta)$ are respectively the bond-stretching and angle-bending terms given in reference [12]. V_t is the individual torsional term of equation (22) for model 1, while for model 2 it should be replaced by $V_t^{\rm cis}$ or $V_t^{\rm trans}$ of equation (23) for the two $\omega_{\rm cis}$ and the two $\omega_{\rm trans}$ respectively. In equation (31), the deformation energy, E_d, becomes an analytic function of z through the explicit dependence on z of the bonds d', the angles θ_1, θ_2 and the dihedral angles $\omega_{\rm cis}^{(1)}$, $\omega_{\rm trans}^{(1)}$, $\omega_{\rm cis}^{(2)}$, $\omega_{\rm trans}^{(2)}$.

In Figure 10, we show the deformation energy E_d, analytically calculated by the expression of equation (31) for both models 1 and 2, in comparison with the corresponding DFT results. As we see, both models perform equally well and the error between the analytical expressions using the classical potential terms and the ab initio computations does not exceed 0.05 eV for the deformation range shown. There are small differences in their agreement with DFT; for example model 2 seems slightly better for intermediate-size displacements while model 1 for larger ones. However, these small differences are insignificant, validating our preference for model 1 on the basis of its simplicity.

7 Conclusion

In summary, we present a simple torsional force field for graphene and other sp^2 carbon nanostructures. To obtain this potential we performed two sets of DFT calculations by folding two different graphene nanoribbon structures around their middle line. The first set of calculations concerns the folding of an armchair nanoribbon around its middle line, i.e. an armchair axis. The second concerns the folding of a zig-zag nanoribbon around its middle line which is a zig-zag axis.

From the DFT derived deformation energies we isolated the "pure" torsional contribution by removing angle-bending terms with the use of a previously proposed analytical potential energy form [12]. The total torsional deformation energy was then fitted to two different analytic forms (containing two parameters each) that we call models 1 and 2; the first (model 1) is that of equation (8) and does not distinguish torsional angles, while the second (model 2) of equation (9) treats differently *cis* and *trans* torsional angles.

We found that the form of model 1 reduces to one parameter form, equation (22), which was found to be an average of the *cis* and *trans* terms of model 2 that differ not so much from each other, see equation (23). This suggests that the use of two different terms is redundant and the single term of model 1 suffices at a reasonable level of accuracy. Both models reproduce accurately the torsional deformation energy of the folded graphene nanoribbons we considered up to folding angles of the order of 30° (≈0.5 rad).

As an additional validation test we considered the case of the deformation energy due to the vertical displacement z of a single carbon atom over graphene's plane. For this task we used the torsional terms of either model 1 or model 2 combined with the bond-stretching and angle-bending all potential energy terms of reference [12]. For all potential energy terms contributing to the deformation energy, analytic expressions in terms of the displacement z were provided. We found that both models perform equally well in this case with errors not exceeding 0.05 eV for a relatively large range of z, up to 0.4–0.5 Å. The good performance of both models in this case validates our choice for the simpler model 1.

The torsional force field presented here, in combination with the bond-stretching and angle-bending potential terms of reference [12], which were also fitted to DFT results using the same density functional approximation, provide a complete, accurate, but simple in form atomistic potential, which is computationally efficient due to its simplicity. Thus, we expect that it will be proven a very useful tool for large scale atomistic simulations of graphene and other sp^2 carbon nanostructures.

We acknowledge helpful discussions with E.N. Koukaras. The research leading to the present results has received funding from Thales project "GRAPHENECOMP", co-financed by the European Union (ESF) and the Greek Ministry of Education. NNL acknowledges support by the project "Advanced Materials and Devices" (MIS 5002409), implemented under the "Action for the Strategic Development on the Research and Technological Sector", funded by the Operational Programme "Competitiveness, Entrepreneurship and Innovation" (NSRF 2014-2020) and co-financed by Greece and the European Union (European Regional Development Fund) and EU H2020 ETN project Enabling Excellence Grant Agreement 642742. G.D.C. acknowledges funding from the General Secretariat for Research and Technology (GSRT) and the Hellenic Foundation for Research and Innovation (HFRI).

Author contribution statement

G. Kalosakas and N.N. Lathiotakis conceived the project. G.D. Chatzidakis and N.N. Lathiotakis did the analytic calculations and the fits. N.N. Lathiotakis, G.D. Chatzidakis, and Z.G. Fthenakis performed the DFT calculations and validation tests for the potential. Finally, N.N. Lathiotakis, G. Kalosakas, and G.D. Chatzidakis prepared the graphics and wrote the first version of the present manuscript which was revised and approved by all authors.

References

1. K.S. Novoselov, A.K. Geim, S.V. Morozov, D. Jiang, Y. Zhang, S.V. Dubonos, I.V. Grigorieva, A.A. Firsov, Science **306**, 666 (2004)
2. A.H. Castro Neto, F. Guinea, N.M.R. Peres, K.S. Novoselov, A.K. Geim, Rev. Mod. Phys. **81**, 109 (2009)
3. L. Chen, Y. Hernandez, X. Feng, K. Mullen, Angew. Chem. Int. Ed. **51**, 7640 (2012)
4. A.C. Ferrari et al., Nanoscale **7**, 4598 (2015)
5. C. Daniels, A. Horning, A. Phillips, D.V.P. Massote, L. Liang, Z. Bullard, B.G. Sumpter, V. Meunier, J. Phys.: Condens. Matter **27**, 373002 (2015)
6. Y.-M. Lin et al., Science **332**, 1294 (2011)
7. F.V. Kusmartsev, W.M. Wu, M.P. Pierpoint, K.C. Yung, in *Applied spectroscopy and the science of nanomaterials*, edited by P. Misra, (Springer, Singapore, 2015)
8. K. Celebi et al., Science **344**, 289 (2014)
9. M.F. El-Kady, Y. Shao, R.B. Kaner, Nat. Rev. Mater. **1**, 16033 (2016)
10. C. Lee, X. Wei, J.W. Kysar, J. Hone, Science **321**, 385 (2008)
11. G. Tsoukleri, J. Parthenios, K. Papagelis, R. Jalil, A.C. Ferrari, A.K. Geim, K.S. Novoselov, C. Galiotis, Small **21**, 2397 (2009)
12. G. Kalosakas, N.N. Lathiotakis, C. Galiotis, K. Papagelis, J. Appl. Phys. **113**, 134307 (2013)
13. A. Fasolino, J.H. Los, M.I. Katsnelson, Nat. Mater. **6**, 858 (2007)
14. K.V. Zakharchenko, M.I. Katsnelson, A. Fasolino, Phys. Rev. Lett. **102**, 046808 (2009)
15. P. Liu, Y.W. Zhang, Appl. Phys. Lett. **94**, 231912 (2009)
16. Z. Xu, M.J. Buechler, ACS Nano **4**, 3869 (2010)
17. M. Neek-Amal, F.M. Peeters, Phys. Rev. B **82**, 085432 (2010)
18. M. Neek-Amal, F.M. Peeters, Appl. Phys. Lett. **97**, 153118 (2010)
19. X. Tan, J. Wu, K. Zhang, X. Peng, L. Sun, J. Zhong, Appl. Phys. Lett. **102**, 071908 (2013)

20. Z. Qi, D.A. Bahamon, V.M. Pereira, H.S. Park, D.K. Campbell, A.H. Castro Neto, Nano Lett. **13**, 2692 (2013)
21. A.P. Sgouros, G. Kalosakas, M.M. Sigalas, K. Papagelis, RSC Adv. **5**, 39930 (2015)
22. E.N. Koukaras, G. Kalosakas, C. Galiotis, K. Papagelis, Sci. Rep. **5**, 12923 (2015)
23. A.P. Sgouros, G. Kalosakas, C. Galiotis, K. Papagelis, 2D Mater. **3**, 025033 (2016)
24. J. Tersoff, Phys. Rev. Lett. **61**, 2879 (1988)
25. J. Tersoff, Phys. Rev. B **37**, 6991 (1988)
26. D.W. Brenner, Phys. Rev. B **42**, 9458 (1990)
27. L. Lindsay, D.A. Broido, Phys. Rev. B **81**, 205441 (2010)
28. J.H. Los, A. Fasolino, Phys. Rev. B **68**, 024107 (2003)
29. J.H. Los, L.M. Ghiringhelli, E.J. Meijer, A. Fasolino, Phys. Rev. B **72**, 214102 (2005)
30. S.J. Stuart, A.B. Tutein, J.A. Harrison, J. Chem. Phys. **112**, 6472 (2000)
31. D. Wei, Y. Song, F. Wang, J. Chem. Phys. **134**, 184704 (2011)
32. Z.G. Fthenakis, G. Kalosakas, G.D. Chatzidakis, C. Galiotis, K. Papagelis, N.N. Lathiotakis, Phys. Chem. Chem. Phys. **19**, 30925 (2017)
33. P. Giannozzi et al., J. Phys.: Condens. Matter **21**, 395502 (2009)
34. A. Dal Corso, http://www.quantum-espresso.org/wp-content/uploads/upf_files/C.pbe-rrkjus.UPF